

Line creep in paper peeling

Jari Rosti, Juha Koivisto, Xavier Illa, and Mikko J. Alava

Department of Engineering Physics, Helsinki University of Technology,

FIN-02015 HUT, email: firstname.secondname@tkk.fi

Paola Traversa and Jean-Robert Grasso

Université Joseph Fourier, CNRS, LGIT, BP 53, 38041 Grenoble, France

Abstract

The dynamics of a "peeling front" or an elastic line is studied under creep (constant load) conditions. Our experiments show an exponential dependence of the creep velocity on the inverse force (mass) applied. In particular, the dynamical correlations of the avalanche activity are discussed here. We compare various avalanche statistics to those of a line depinning model with non-local elasticity, and study various measures of the experimental avalanche-avalanche and temporal correlations such as the autocorrelation function of the released energy and aftershock activity. From all these we conclude, that internal avalanche dynamics seems to follow "line depinning" -like behavior, in rough agreement with the depinning model. Meanwhile, the correlations reveal subtle complications not implied by depinning theory. Moreover, we also show how these results can be understood from a geophysical point of view.

PACS numbers:

I. INTRODUCTION

Creep is one of the fascinating topics in fracture for a physicist: the deformation and final fracture of a sample follow empirical laws with a rich phenomenology. It is expected that there are similarities and differences with "static" fracture encountered in brittle materials such that so-called "time-dependent rheology" is not relevant [1]. However, the phenomenon of creep is visible in most any setting regardless of whatever a tensile test might indicate about the typical material response. A particular scenario where one can study creep is the advancement of a single crack under a constant driving force. One can study this in simple paper sheets, and for quite some time it has been noticed that this involves statistical phenomena, an intermittent response which could be characterized by "avalanches", in particular of acoustic emission (AE) events [2, 3, 4, 5].

A particular experiment we analyze in this work is related to the dynamics of a *crack line* as it moves through a sample, largely constrained on a plane. This can be achieved in the case of paper in the so-called Peel-In-Nip (PIN) geometry (see below for a description). The tensile case has been already reported in Ref. [6] and an early account of the creep results published as Ref. [7]. The mathematical description of the line is a crack position $h(x, t)$, where h is the position coordinate along the direction of line propagation and x is the coordinate perpendicular to h . On the average, the crack moves with the *creep velocity* v ($\bar{h} = vt$).

The problem has here, as in other such examples (the Oslo plexiglass experiment [9, 10]), three important ingredients: randomness in that the peeling line experiences a disordered environment coming from the fiber network structure, a driving force K_{eff} or a stress intensity factor, and the self-coupling of the interfacial profile h . In this particular problem, it takes place via a long-range elastic kernel [11], expected to scale as $1/x$ or as k in Fourier space.

For a constant force K_{eff} the dynamics exhibits a depinning transition, of non-equilibrium statistical mechanics. This implies a phase diagram for $v(K_{eff})$. The crack begins to move ($v > 0$) at a critical value K_c of K_{eff} such that for $K_{eff} > K_c$. In the proximity of K_c the line geometry is a self-affine fractal with a roughness exponent ζ . The planar crack problem [12, 13] has been studied theoretically via renormalization group calculations and numerical simulations, and via other experiments as noted above. The roughness exponent

of theory $\zeta_{theory} \sim 0.39$ has traditionally been considered to be absent from experiments [8, 9, 10, 14], but recent results of Santucci et al. imply that the regime might be visible upon coarse-graining. Imaging experiments prove in that case that as expected the line moves in avalanches, and the avalanche size s distribution seems to have the form $P(s) \sim s^{-1.6 \dots -1.7}$ [9, 10].

Here we look at the scenario of creep for the PIN geometry. This subject is such that ordinary "fracture creep" and the particular scenario related to depinning transitions coincide. The creep of elastic lines becomes important for $K_{eff} \leq K_c$ since thermally assisted movement due to fluctuations takes place with a non-zero temperature [15, 16, 17]. In usual depinning, it is assumed that thermal fluctuations nucleate "avalanches" which derive their properties from zero-temperature depinning, and the avalanches then translate into a finite velocity $v_{creep} > 0$. There are two interesting differences in the fracture line creep to other such in depinning. First, the line elasticity is non-local, and second, in materials (such as paper here) where there is no healing, the line motion is irreversible, there are no fluctuations in metastable states as in the case of magnetic domain walls, for instance.

In this scenario, the creep velocity becomes a function of the applied stress intensity factor and the temperature, $v_{creep} = v_{creep}(K_{eff}, T)$. As creep takes place via nucleation events over energy barriers [15], the description of those barriers is of fundamental importance. One can show by scaling arguments and more refined renormalization group treatments that the outcome has the form of the following creep formula

$$v_{creep} \sim \exp(-C/K_{eff}^\mu). \quad (1)$$

This gives the relation to the driving force K_{eff} using the creep exponent, μ . The value of the exponent depends on the elastic interactions and the dimension of the moving object (a line), and we expect

$$\mu = \theta/\nu = \frac{1 - \alpha + 2\zeta}{\alpha - \zeta}. \quad (2)$$

The exponents θ , ν , and ζ denote the energy fluctuation, correlation length, and *equilibrium* roughness exponents. All these exponents are functions of α , the k -space decay exponent of the elastic kernel. For long range elasticity, one would assume $\alpha = 1$.

The fundamental formula of Eq. (2) has been confirmed in the particular case of 1+1-dimensional domain walls and other experiments [18, 19]. We have ourselves reported on results, which show an inverse exponential dependence of $v_{creep}(m) \sim \exp(-1/m)$, where

m is the applied mass in the experiment (see below), as is appropriate for non-local line elasticity with an *equilibrium roughness exponent* of $\zeta = 1/3$. In the current work we go further by two important steps. First, we consider creep simulations of an appropriate non-local line model and compare the avalanche statistics and $v(m)$ to those from the experiments (see Fig. 1 for an example of the activity timeseries from an experiment and a simulation). Then, we ask the fundamental question: what can be stated of the correlations? This relates to the timeseries of released energy, to aftershock rates and we present extensive evidence. The experimental signatures show subtle correlations that are rather different from what one would expect from the (depinning) creep problem with non-existing avalanche to avalanche correlations.

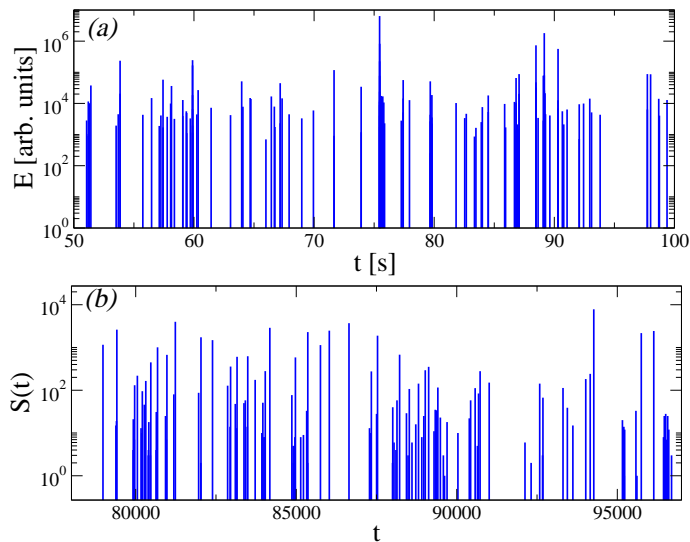


FIG. 1: Activity as a function of time inside a given time window (a) for the creep experiment with 410g load, and (b) for simulations with $f = 1.87$ and $T_p = 0.002$. In both cases we neglect the duration of the avalanche and we only take into account the starting time and the size of each avalanche, obtaining a data series $\{t_i, E_i\}$ for the experiments and $\{t_i, S_i\}$ for simulations (definition of S_i is given in Section II B)

The structure of the rest of the paper is as follows. In the next Section, we discuss the experimental setup and the simulation model. Section III shows results on $v(m)$ both from experiment and simulation. In Section IV we present data on avalanche statistics again comparing the two cases. Section V offers an extensive analysis of correlations by using a number of techniques to look at the experiment. Finally, Section VI finishes with

Conclusions and a Discussion.

II. METHODS

A. Experiment

In Figure 2 we show the apparatus [6]. The failure line can be located along the ridge, in the center of the the Y-shaped construction formed by the unpeeled part of the sheet (below) and the two parts separated by the advancing line. Diagnostics consist of an Omron Z4D-F04 laser distance sensor for the displacement, and a standard plate-like piezoelectric sensor [6]. It is attached to the setup inside one of the rolls visible in Fig. 2, and the signal is filtered and

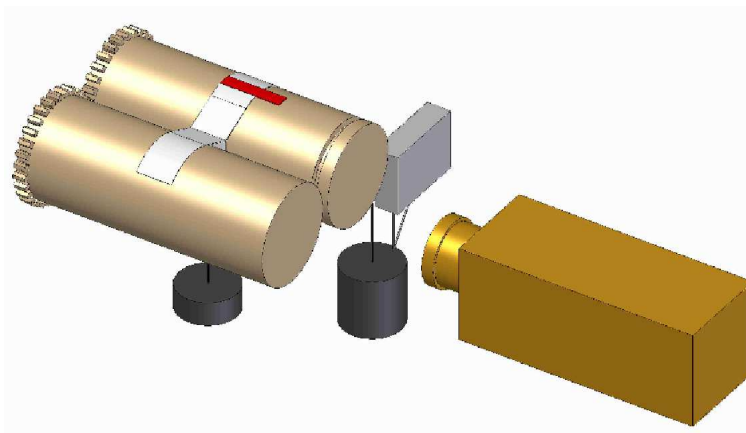


FIG. 2: Experimental setup for peeling experiment. The paper (white) is peeled between two cylinders (copper) separated by a few millimeters. The driving force is generated by a larger hanging weight (black). A smaller weight adjusts the peeling angle. The AE and distance data are collected by piezo transducer (red) and a laser sensor (gray).

amplified using standard techniques. The data acquisition card gives us four channels at 312.5 kHz per channel. We finally threshold the AE data. The displacement data is as expected highly correlated with the corresponding AE, but the latter turns out to include much less noise and thus convenient to study. For paper, we use perfectly standard copy paper, with an areal mass or basis weight of 80 g/m^2 . Industrial paper has two principal directions, called the “Cross” and “Machine” Directions (CD/MD). The deformation characteristics are much more ductile in CD than in MD, but the fracture stress is higher in MD [20]. We

tested a number of samples for both directions, with strips of width 30 mm. The weight used for the creep ranges from 380 g to 450 g for CD case and from 450 g to 533 g for MD case. The mechanical (and creep) properties of paper depend on the temperature and humidity. In our setup both remain at constant levels during experiments, and the typical pair values for environment is 40 rH and 26 °C.

B. Simulations

We want to simulate the evolution of a discrete long-range elastic line of size L in a disordered media. The line is characterized by a vector of integer heights $\{h_1, \dots, h_L\}$ with periodic boundary conditions, although the experiment does not present periodic bound conditions.

The long-range elastic force [21] acting on a string element is given by

$$f_i^{elastic} = k_o \left(\frac{\pi}{L}\right)^2 \sum_{\substack{j=1 \\ j \neq i}}^L \frac{h_j - h_i}{\sin\left(\frac{x_j - x_i}{L} \pi\right)}, \quad (3)$$

where all forces on all sites can be computed in a $L \log L$ operations using a fast-Fourier-transform (FFT) algorithm [22]. Simulations are done using $k_o = 0.01$ and $L = 1024$. The random force due to the quenched disorder may be obtained from a standard normal distribution, i.e a Gaussian distribution with zero mean and a variance of one $f_i^{random} = N(0, 1)$. Then, the total force acting in a given element of the string is $f_i = f_i^{elastic} + f_i^{random} + f$, where f is the external applied force.

At this point, we need to introduce a dynamics which mimic the experiment evolution. A basic characteristic of the experiment is that it is completely irreversible, so the dynamics has to include this important feature. We consider a discrete time evolution and the discrete dynamical rule [22] is given by:

$$h_i(t+1) - h_i(t) = v_i(t) = \theta[f_i] \quad t = 0, 1, 2 \dots \quad (4)$$

where θ is the Heaviside step function. Then we apply the following procedure:

1. Start at $t = 0$ with a flat line located at $h = 0$ setting $h_i = 0 \quad \forall i$.
2. Compute the local force (f_i) at each site and using the dynamical rule (Eq. 4) compute the local velocity of each site. We can define the velocity of the string for this time, as $v(t) = \frac{1}{L} \sum_{i=1}^L v_i(i)$.

3. Advance the sites according their local velocities v_i .
4. Generate new random forces for those sites that have been advanced.
5. Go to step (2) and advance the *simulation time* by one unit.

This evolution shows a depinning transition at $f_c \sim 1.88$ in which the velocity of the line $v(t \rightarrow \infty) > 0$ when $f > f_c$ and $v(t \rightarrow \infty) = 0$ when $f < f_c$.

In order to simulate the creep evolution of the string we use an external force below the depinning threshold, and when the line gets stuck we let thermal fluctuations play a role. We scan all the sites and set $v_i(t) = 1$ with a probability $p = \exp\left(\frac{f_i}{T_p}\right)$ and $v_i(t) = 0$ with a probability $1 - p$, where T_p is proportional to temperature. This can trigger an avalanche which will have a finite duration T since the system is below the depinning threshold. We define the avalanche size as $S = \sum_T v(t)$. If we consider small enough temperatures compared to the typical internal forces, the avalanche needs some time to be triggered, which is defined as the waiting time τ . We define this waiting time as the time between the end of an avalanche and the starting time of the next one.

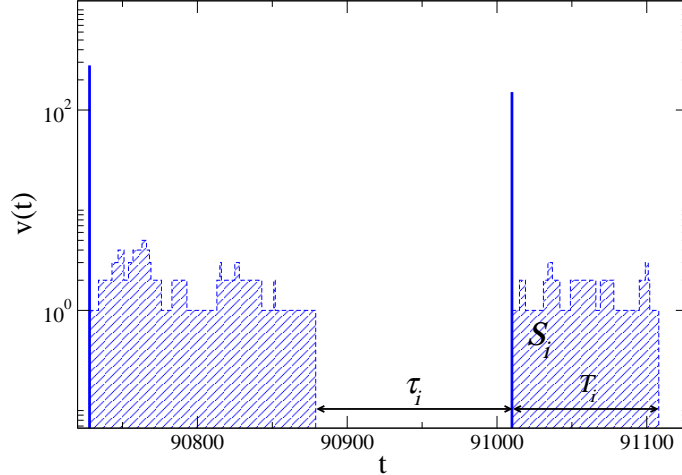


FIG. 3: Velocity of the long-range elastic string as a function of simulation time (dotted line). The vertical and solid lines represents the signal $S(t)$ plotted in figure 1(b). Avalanche properties are also shown: τ_i is the waiting time, T_i is the avalanche duration duration, and S_i is the avalanche size.

In summary, this long-range elastic line model in the creep regime has an avalanche-like behaviour. Each avalanche is characterized by three quantities: Waiting time τ , duration

T , and size S (see Fig. 3). Moreover, we observe that for long times, when the steady state is reached, durations are small compared to waiting times, for that reason we can simplify the signal just taking into account the starting time of the avalanche and its size.

III. CREEP VELOCITY

The main data about both simulations and experiment on the creep velocity are shown in Figure 4. The prediction of Eq. (1) is that the velocity is exponential in the effective driving force. In the case of the experiments at hand, we face the problem that we do not know the average fracture toughness $\langle K \rangle$ empirically. It depends on the loading geometry, and on the material at hand. There are estimates for similar papers in the literature in the mode I case (see e.g. Ref. [23]) which indicate that the value of $\langle K \rangle$ is lower by at least a factor of two compared with the actually used loads. One can try to work around the problem by guessing $\langle K \rangle$ and checking how that affects the apparent functional relationship of v vs. the reduced mass $m_{eff} = m - \langle K \rangle$. In the range of physically sensible values of $\langle K \rangle$ the velocity exponential behaviour does not change and thus we can take $m_{eff} = m$.

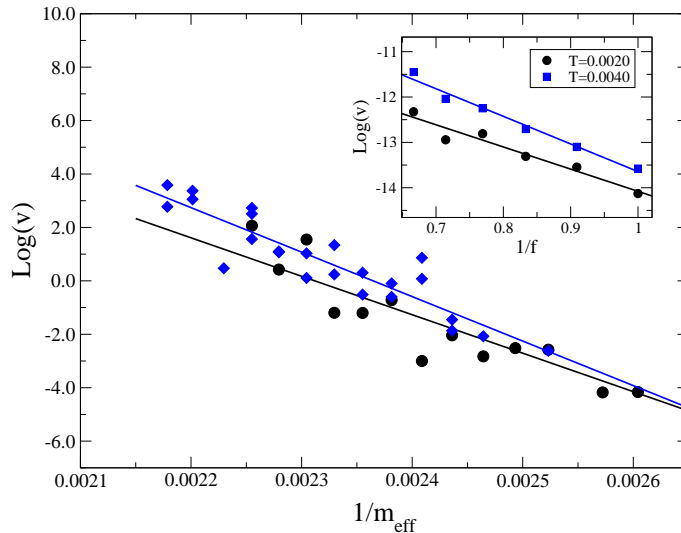


FIG. 4: The creep velocity vs. the inverse of the applied force or mass, $m_{eff} = m$. Inset: creep velocity vs. f for the simulation model for two different temperatures.

From the figure we may conclude that the effective creep exponent $\mu \sim 1$, though there is variability among the data sets. One of the data sets (black circles) shows some slight

curvature. The main finding, interpreted via Eq. (2) then indicates that the effective roughness exponent $\zeta \sim 1/3$, which is the expected *equilibrium* value for a long-range elastic problem with $\alpha = 1$ [7].

The numerical simulation data agree qualitatively with the exponential decay except very close to the depinning transition. According to the creep formula (see e.g. [17]), we should expect that the velocity of the long-range string was

$$v(f, T_p) \sim \exp \left[-\frac{C}{T_p} \left(\frac{1}{f} \right)^\mu \right]. \quad (5)$$

However, it appears that slope as a function of the temperature is not exactly the expected one. One reason is that the model is simplified: we only let thermal fluctuations act when the string gets stuck so avalanche nucleation during an avalanche is neglected. This may be of importance very close to f_c and for long avalanches.

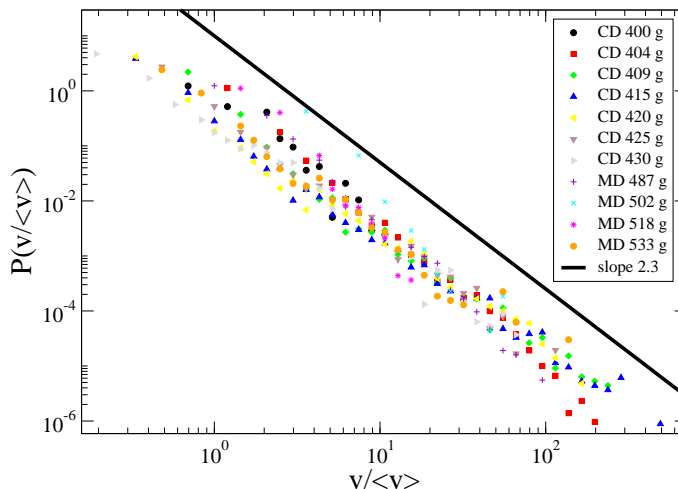


FIG. 5: Histogram of a normalized velocity obtained from discretized distance data. Velocity, v , is an average in a 0.5 s time window. $\langle v \rangle$ is an average over experiments with same weights.

The exponential average creep velocity can most directly be compared with the measured velocities from the distance sensor over short time-spans. Figure 5 shows the probability distributions $P(v)$ for a very large number of different experiments, for the $v = \Delta h / \Delta t$ with $\Delta t = 0.5$ s. The general trend shows clear stick-slip characteristics in the sense that the local velocities vary with a power-law -like fashion. The typical slope of the data is about -2.3 though a more detailed look indicates that there is a tendency for the exponent to change with m and with Δt (increasing both decreases the slope). It is an interesting question

of how this locally time-averaged velocity is related to the average creep velocity, and the avalanches that contribute to it, somewhat hindered by the relative large fluctuations in the distance sensor - for which reason we resort in the detailed avalanche dynamics studies to the AE.

IV. STATISTICAL DISTRIBUTIONS

Next we consider the statistics of the AE timeseries from the experiments as signatures of the intermittent avalanche activity in the system during creep. In our setup, we face the problem that direct imaging of the front dynamics is if not impossible then difficult to realize. Thus we take the AE data up to be scrutinized as detailed information. It can be studied from the viewpoint of the correlations of the creep avalanche activity but the finer details thereof are left to the next Section. Here, we consider the averaged distributions of three quantities: i) AE energy E in experiments and avalanche size in simulations assuming that the avalanche energy is proportional to its size $E \sim S$ ii) waiting times τ both for experiments and simulations and iii) avalanche durations T only for simulations, because experimental avalanches have very short durations and can be neglected.

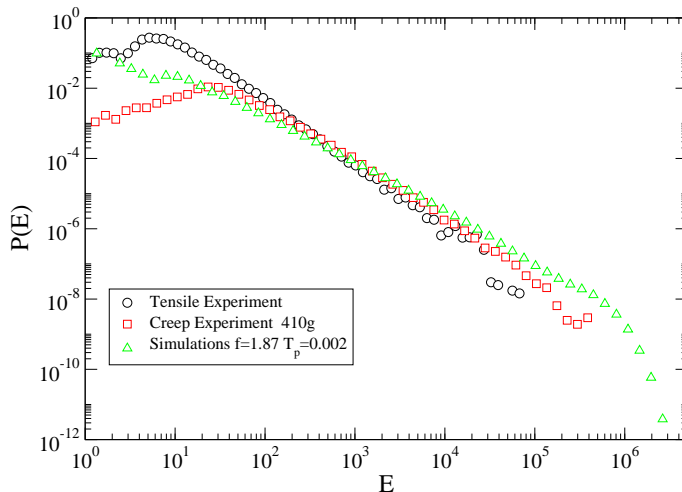


FIG. 6: Energy distributions for the tensile experiment (circle), for the creep experiment (square), and for the simulations (triangle up). For the simulations we are plotting the histogram of the avalanches sizes $\{S_i\}$. We can consider that the energy of an avalanche is proportional to its size, so $S_i \sim E_i$.

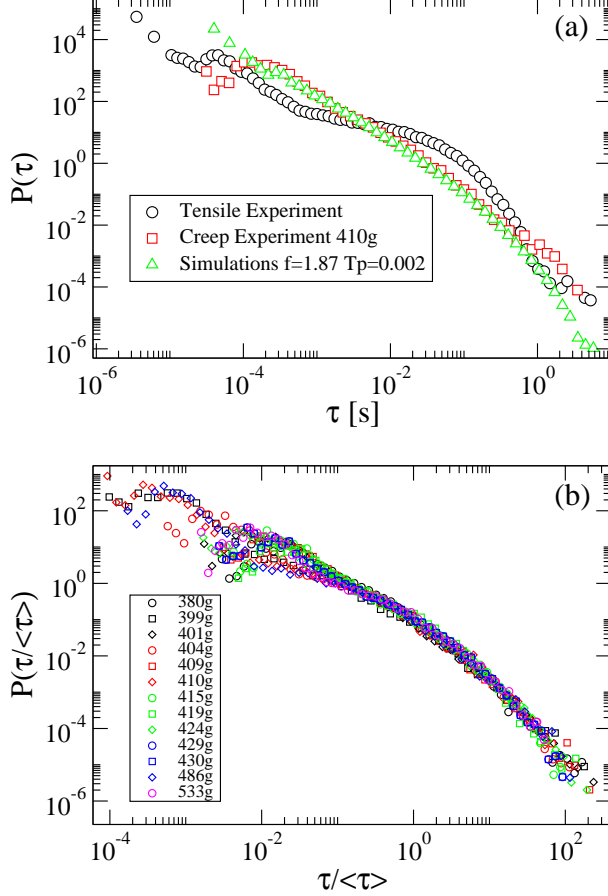


FIG. 7: (a) Waiting time distributions for the tensile experiment (circle), for creep experiment with 410g (squares), and for the simulations with $f = 1.87$ and $T = 0.0020$ (triangles up). (b) Normalized waiting times for different creep experiments.

Figure 6 shows three cases of the avalanche size distributions. We compare the creep data for one mass m to a similar dataset for a tensile experiment done at a constant average front velocity [6]. Moreover data is included from the creep model for the parameters shown in the caption. The normalization of the data for the experiments is such that the E_{min} has been scaled to unity. Recall that the events are restricted in size from below by a thresholding applied to the original AE amplitude signal $A(t)$, from which the events are reconstructed. We can observe that the effective power-law exponents of the experimental data are ~ 1.6 for the creep and ~ 1.8 for the tensile cases, respectively. These are very close to each other, while the simulation data results imply ~ 1.4 not very far from the experimental values. We also can observe that there is no evident cutoff in any of them (the bending in the

simulations case is a finite size effect). These data can be compared with the Oslo plexiglass experiment where for the avalanche size distribution the value of $\beta = 1.6 \pm 0.1$ has been found [9, 10].

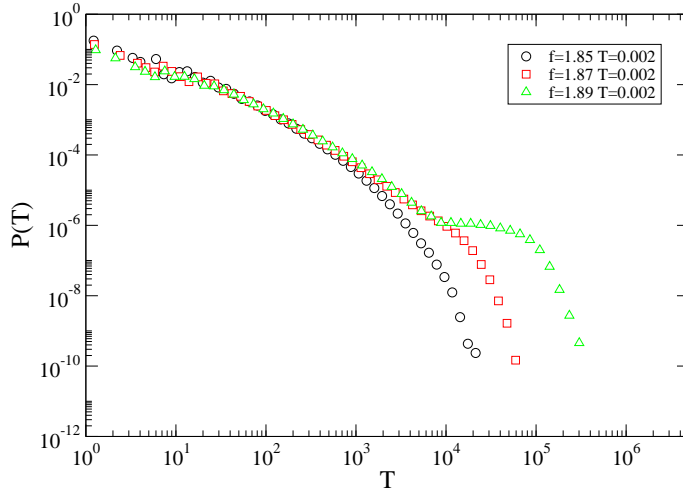


FIG. 8: Avalanche duration distributions for $Tp = 0.002$ and three different forces. For the case with $f = 1.89$ we are above the depinning threshold.

The waiting times are reported in Fig. 7. For all the three cases $P(\tau)$ is broad. In the tensile case, it is known that there appears to be a "bump" in the distribution, or a typical timescale. This is absent from the creep one. It is interesting to note that here the simulation model agrees rather well with the creep case. For larger m it is possible that the waiting times start to look more like the tensile case. We also present the scaled distributions for all the experiments. Later, in the next section, we discuss the attempt to link this to a background plus correlated, triggered activity.

Finally, in Fig. 8 we show the avalanche durations from the simulations. In the case of the experiment this is more complicated due to the fact that the actual amplitude signal is convoluted via the preprocessing electronics and the response function of the piezos with which the AE is measured. Later we present some examples of the outcome, but here we just discuss the clear-cut case of the simulations also since they give an idea about what one might see in the experiment, ideally. The main points that one learns from the Figure are that a true power-law-like $P(T)$ ensues only at the proximity of the f_c . For values higher or lower than that the shape of the distribution changes, in particular such that not only a cut-off appears but also the clear power-law character starts to disappear.

V. MEASURES OF CORRELATED DYNAMICS

A. Correlations

Next we look at the detailed temporal structure of the AE signal. The main question is whether the creep activity exhibits interesting features that would in particular differ from the theoretical expectations - based on elastic line depinning the inter-avalanche correlations should be expected to be negligible.

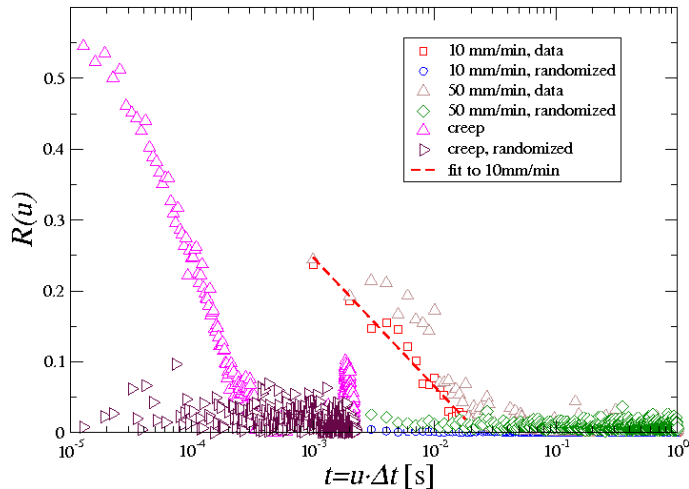


FIG. 9: The autocorrelation function of the averaged event energy in paper peeling under creep and tensile loading modes. Comparisons to the randomized data are also included. The numerical data and the corresponding randomized data are not distinguishable.

In Figure 9 we show the autocorrelation function $R(t)$ of the event energy time series. The autocorrelation function is defined as:

$$R(u) = \frac{\frac{1}{N} \sum_{t=1}^N E_t E_{t+u} - \langle E \rangle^2}{\langle E^2 \rangle - \langle E \rangle^2} \quad (6)$$

where E_t is the energy of the AE signal at time t and $\langle E \rangle$ is the average value of the energy. E_t is defined as a sum of squared amplitudes of the AE signal in the time interval $[t, t + \Delta t]$. The length of the interval Δt is chosen to be $10^{-3}s$ in the tensile and $10^{-5}s$ in the creep peeling experiment in order to capture the correlations in both cases.

When compared to paper peeling experiments under a constant strainrate, the correlation decays at a much faster rate than in creep peeling experiments. In that case, the existence

of a slow decay might be taken to be connected to the fact that there is a typical scale in the waiting time distribution which is not the case for creep, seemingly. The functional form of the shown case of a logarithmically decreasing autocorrelation function is $R(t) = -0.3 - 0.08 \ln(t)$. The data are also compared to a randomized timeseries, and one can see that the correlations disappear. For the simulated data the autocorrelation function shows no difference to a randomized signal. All in all these results imply that there are contrary to theoretical models temporal correlations, albeit in creep on a very short timescale.

In Figure 10 we show an envelope event form for different events with different event energies. We see an exponential decay for the tail of the event, but the event envelope becomes more extended in time when the energy of the event is larger. Typical events extend up to 0.5ms, which corresponds to decay of the correlation in the Fig. 9. A correlation up to time-scales larger than the typical event length is only seen in the strain-controlled peeling.

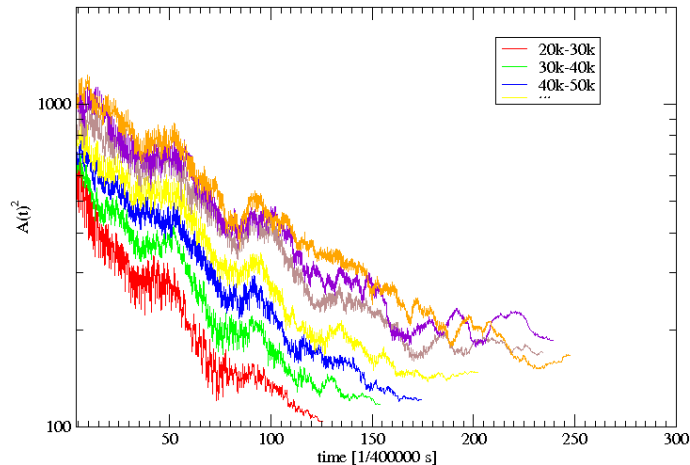


FIG. 10: Squared amplitude of an event averaged over all events in the creep peeling experiment. The average is taken over events with different sizes and the size is indicated as different colors in the figure.

Since the timeseries of AE is so intermittent it is better to concentrate on measures that consider directly the avalanches. In Figure 11 we depict the averaged energy as a function of a silent time before the event from paper peeling experiments in creep. The event energy is in many datasets slightly correlated to the waiting time before the event. This correlation disappears if one considers the opposite case of the waiting time after the

event. The suggested interpretation is that the elastic fracture line apparently as a physical system ages before a large event, while there is no real dependence of the waiting time on the energy dissipated in the previous event.

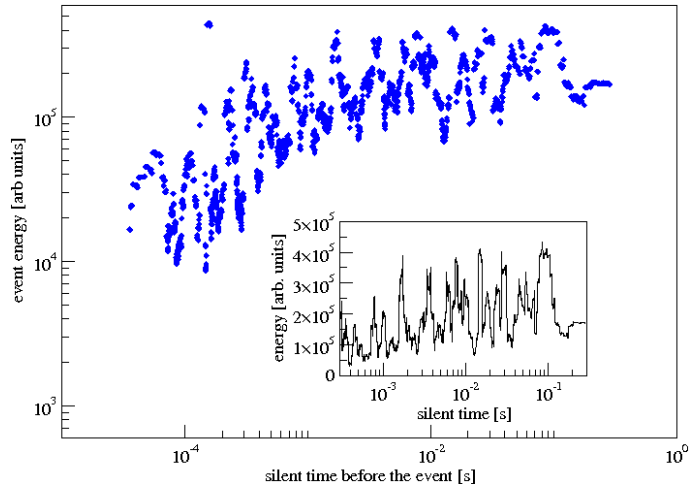


FIG. 11: Averaged energy as a function of silent time before the event with weight 410g.

The difference in the autocorrelation between the creep and tensile peeling experiments might be attributed to the forcing the line to move in the latter, which induces a “fiber-scale” to results. This is also supported by observing the waiting time distribution, where the pdf deviates from a power-law.

In paper peeling we study the clustering of events by computing the correlation integral $C(\Delta T)$, that is the probability that two events are separated smaller time than ΔT . The correlation integral is given by:

$$C(\Delta T) = \frac{2}{N(N-1)} \sum_{i < j} \theta[\Delta T - (t_j - t_i)], \quad (7)$$

where N is number of events in the experiment and t_i is the event occurrence time.

Correlation integrals [24] are shown in the Fig. 12 for the peel creep experiment. If the probability of the event occurrence is equal for every time interval, then one can assume that correlation integral increases as $C(\Delta T) \sim \Delta T$. We see a power law $\Delta T^{0.9}$ in sufficiently large times, but when the distance of events approaches the experiment length we see small deflection in the curve. At temporal scales of the order of 10^{-2} s we see deviation from the power law behaviour, which indicates event clustering.

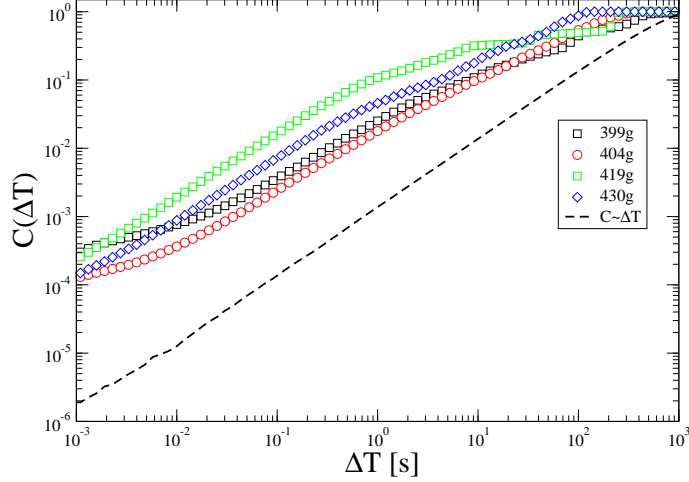


FIG. 12: Correlation integrals for the creep in peeling experiment.

B. Seismicity - cascading occurrences as a model for the experimental data

In this part we will show how fracture in heterogeneous material, such as line creep in paper peeling, behaves, in time, similarly to the rupture at the Earth scale, e.g. the earthquakes driven by plate tectonic deformation.

From seismology it is known that seismicity can be described by two processes: the background seismicity and the triggered events. The first one is modelled as a homogeneous Poisson process, while the second one as a power law decay of seismic rate following the occurrence of any event, e.g. the Omori's law [25, 26, 27]:

$$R = \mu_0 + \sum_{t < t_i} \lambda_i(t) \quad (8)$$

The first term in the right hand side of Eq. 8 is the background seismicity, while the second term is the correlated part of the seismicity, that is, the superposition of time-dependent series of triggered seismicity following any event. The triggering process of the latter is reproduced by models of cascading effect for earthquake interactions, i.e. ETAS (Epidemic Type Aftershock Sequence) model [25, 26, 28]. This stochastic point process is based on the Gutenberg-Richter law for energy distribution and Omori's law for time distribution of seismicity rate. According to this model, the rate of aftershocks triggered by an earthquake occurring at time t_i with magnitude M_i is given by:

$$\lambda_i(t) = \frac{K_0}{(c + t - t_i)^p} 10^{\alpha(M_i - mc)}, \quad (9)$$

where K_0 , α , c and p are constants and mc is the completeness magnitude of the catalogue.

The total earthquake rate of Equation (8) is therefore the sum of all preceding earthquakes (triggered directly by the background events or indirectly by previous triggered events) and the constant background rate μ_0 . This model reproduces most of the statistical properties of earthquakes, including aftershock and foreshocks distributions in time, space and energy [27].

Figure 13 illustrates the average acoustic event rate following any event for the peel creep experiments (load $m = 409g$). It is reminiscent of Omori’s law for tectonic seismicity, where we can observe the power law decay representing the cascade of aftershocks following an event. For times greater than 10^{-2} seconds, the event rate keeps constant, at the background rate level. The exponent of the power law decay of event rate is equal to 1.5 ± 0.1 . This is fairly close to what would fit the experimental $P(\tau)$ demonstrated in Fig. 7.

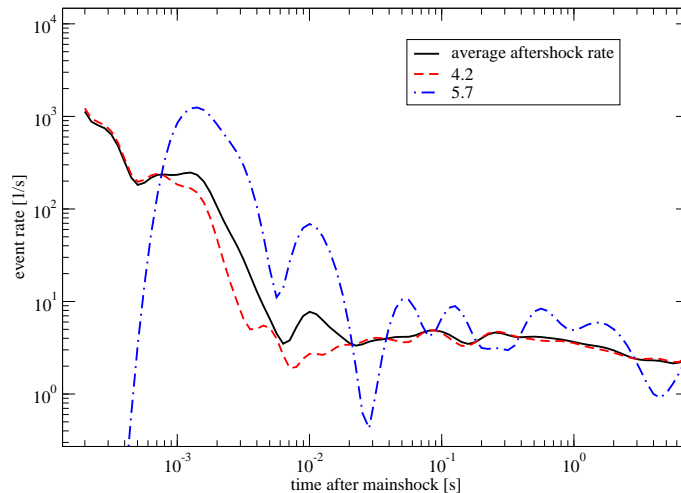


FIG. 13: Event rate following events in paper peel creep experiments with $m = 409g$. Time $t = 0$ is the target event occurrence. Aftershock rates are averaged within each magnitude class of target event (blue line: 4.2 – 5.72; red line 5.72 – 7.2). We compute the magnitude class $M = \log_{10}(E_M)$ where E_M is the energy of the target event. All magnitude classes are averaged together (thick black line). Correlation between events is characterized by a power law decay of the activity after the target event. The time for which events are correlated is a function of the target event magnitude, as well as the number of triggered events (see Equations (8) and (9)). The observed duration of the aftershock sequence is bounded by the level of the background uncorrelated constant rate.

The AE, triggered by line creep in paper peeling, is characterized by power law distri-

bution on energy (Fig. 6) and power law relaxation of aftershock rate (Fig. 13). ETAS style models reproduce these macroscopic patterns, including foreshocks as aftershocks of conditional mainshocks [28]. Corral [29] shows that the inter-event time probability density for such kind of ETAS model for event occurrences follows a gamma distribution, according to:

$$p(\tau) = C\tau^{\gamma-1} \exp(-\tau/\beta) \quad (10)$$

where τ is the normalized inter-event time obtained by multiplying the inter-event time δt with the earthquake rate λ , that is $\tau = \delta t\lambda$.

Molchan [30] showed that, in agreement with Equation (10), the distribution decays exponentially for large inter-event times and that the value $1/\beta$ is the fraction of mainshocks among all seismic events. According to Hainzl et al. [31], $1/\beta$ is a regional quantity, allowing for non-parametric estimate of the background rate in a specific process. In order to simulate the AE properties of the creep fracture experiment ($m = 409g$), we tuned an ETAS model to fit the estimated percentage of background activity of real data. One must notice that robust inversion of ETAS model parameters is not yet available. Figure 14 shows the comparison between inter-event time distributions of a synthetic catalogue generated by ETAS model. Both, simulations and data inter-event time distributions fit a gamma distribution. Other possible data fittings are possible [32], but this lies outside our aim of comparison between data from paper peeling and ETAS simulations. The fit may underestimate here (see also Fig. 7b) slightly the exponent of the power-law part of the waiting-time distribution. In any case, the relevant exponent here is definitely smaller than in the case of rock fracture [33] ($p = 1.4$).

To summarize, line creep in paper peeling at a scale of $\sim 10^{-1}m$ and $\sim 10^2s$ triggers brittle creep damage that seems to share the same generic temporal properties than the ones observed for tectonic seismicity at scales of $\sim 10^6m$, $\sim 10^2$ years. These properties can be reduced to a rough constant seismicity rate with bursts of correlated activity, contemporary to power law distribution of event sizes and (short-time) inter-event times. Estimates of Omori's law exponent suggest a faster relaxation for the paper peeling case than for Earth crust response to tectonic loading, p equal to 1.4 and 1 respectively [26]. The portion of uncorrelated events suggests a slightly lower triggered event rate in paper peeling than in the Earth crust deformation. Estimations of the background portion of AE did not show any sensitive dependence on the applied loading. Whether the difference between paper

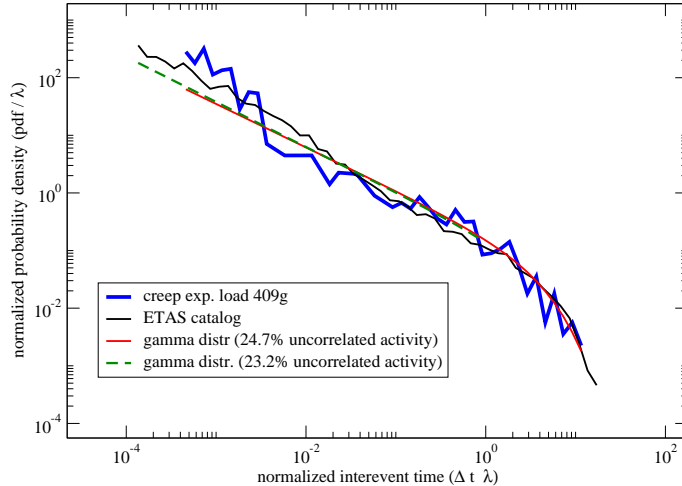


FIG. 14: Inter-event time probability distribution for experimental dataset (thin red curve) and synthetic catalogue generated by ETAS model (thin black curve). Dotted thick curves are gamma distribution fits to data and ETAS model (red dotted line for the real data and black dotted curve for ETAS). Estimations of background fraction of events according to Hainzl et al. (2006) technique are close together (23 – 25%) for both data and simulation. ETAS parameters are: $p = 1.4$, $K_o = 0.09$, $\alpha = 0.9$ ($n = 0.9$), $b = 1$, $c = 0.001s$.

experiments and earthquakes come from experimental conditions or fracturing mode (i.e. tensile, creep or compression) remains an open question. For earthquakes no change in relative portions of background and triggered activity is resolved for compression, extensional or shear tectonic settings.

VI. CONCLUSIONS

We have overviewed a simple creep experiment which uses paper and can be studied to investigate planar crack propagation in a disordered medium. The information that one can obtain and then compare to relevant theory extends from the average front velocity to details of the spatiotemporal dynamics. We have also for a comparison studied a classical non-local elastic line model under creep conditions. This shows similar features to the experiment: an exponential dependence of the creep velocity on the applied force or mass or stress-intensity factor.

The typical statistical distributions are power-law -like in particular for the event en-

ergy/size. It is perhaps useful to recall that the waiting time distribution is quite broad. There is currently no understanding as to why, in particular one should note that the current experimental setup allows to study this issue in a steady-state unlike in most other fracture-related creep tests. In general as such distributions are regarded the line creep model agrees at least qualitatively with the experimental data. Our results are also in line with other similar planar crack data (though these are obtained usually in the constant-velocity ensemble, not in creep [9, 10, 34]).

Looking in more detail at the correlations of the activity, differences transpire however. The experimental AE events show subtle correlations via the autocorrelation function, via the waiting times before events, and via the Omori's law. All these measure different aspects of the avalanche activity, and in all the cases the model differs in its behavior. Here, we lack completely theoretical understanding, in particular as regards such a quantitative measure as the Omori exponent. It is interesting to note that geophysics -oriented analysis methods produce results in agreement with observations from tectonic activity. Here again the steady-state character of the experiment at hand is of utility.

In the future such experiments and such comparisons can be used to study several different aspects of avalanching systems, creep fracture, and models for line depinning. A particularly pertinent question is for instance whether rate-dependent processes in the material at hand modify the kinetics of the creep in some suitable way that still maintains the creep vs. force -relation intact. We shall ourselves attempt a more careful study of the creep model, and analyze how its correlation patterns could be matched with the experiment.

Acknowledgements - The authors would like to thank for the support of the Center of Excellence -program of the Academy of Finland, and the financial support of the European Commissions NEST Pathfinder programme TRIGS under contract NEST-2005-PATH-COM-043386. MJA is grateful for the hospitality of the Kavli Institute of Theoretical Physics, China in Beijing, where the work at hand was to a large degree completed. Discussions with Lasse Laurson (Helsinki), Stéphane Santucci (Oslo), Daniel Bonamy (Saclay), and Stefano Zapperi (Modena) are also acknowledged.

[1] M. J. Alava, P. K. V. V. Nukala, and S. Zapperi, *Adv. Phys.* **55**, 349 (2006).

[2] J. P. Sethna, K. A. Dahmen, and C. R. Myers, *Nature* **410**, 242 (2001).

- [3] J. Kertész, V. K. Horváth, and F. Weber, *Fractals* **1**, 67 (1993).
- [4] L. I. Salminen, A. I. Tolvanen, and M. J. Alava, *Phys. Rev. Lett.* **89**, 185503 (2002).
- [5] S. Santucci, L. Vanel, and S. Ciliberto, *Phys. Rev. Lett.* **93**, 095505 (2004).
- [6] L. I. Salminen, J. M. Pulakka, J. Rosti, M. J. Alava, and K. J. Niskanen, *Europhys. Lett.* **73**, 55 (2006).
- [7] J. Koivisto, J. Rosti, and M. J. Alava, *Phys. Rev. Lett.* **99**, 145504 (2007).
- [8] A. Rosso and W. Krauth, *Phys. Rev. E* **65**, 025101(R) (2002).
- [9] J. Schmittbuhl and K. J. Måløy, *Phys. Rev. Lett.* **78**, 3888 (1997).
- [10] K. J. Måløy, S. Santucci, J. Schmittbuhl, and R. Toussaint, *Phys. Rev. Lett.* **96**, 045501 (2006).
- [11] D. S. Fisher, *Phys. Rep.* **301**, 113 (1998).
- [12] S. Ramanathan and D. S. Fisher, *Phys. Rev. Lett.* **79**, 877 (1997).
- [13] J. Schmittbuhl, S. Roux, J. P. Vilotte, and K. J. Måløy, *Phys. Rev. Lett.* **74**, 1787 (1995).
- [14] A. Rosso and W. Krauth, *Phys. Rev. Lett.* **87**, 187002 (2001).
- [15] T. Nattermann, *Europhys. Lett.* **4**, 1241 (1987); L. B. Ioffe and V. M. Vinokur, *J. Phys. C* **20**, 6149 (1987); T. Nattermann, Y. Shapir, and I. Vilfan, *Phys. Rev. B* **42**, 8577 (1990).
- [16] P. Chauve, T. Giamarchi, and P. Le Doussal, *Phys. Rev. B* **62**, 6241 (2000).
- [17] A. B. Kolton, A. Rosso, T. Giamarchi, and W. Krauth, *Phys. Rev. Lett.* **94**, 047002 (2005).
- [18] S. Lemerle, J. Ferré, C. Chappert, V. Mathet, T. Giamarchi, and P. Le Doussal, *Phys. Rev. Lett.* **80**, 849 (1998).
- [19] Th. Braun, W. Kleemann, J. Dec, and P. A. Thomas, *Phys. Rev. Lett.* **94**, 117601 (2005); T. Tybell, P. Paruch, T. Giamarchi, and J.M. Triscone, *Phys. Rev. Lett.* **89**, 097601 (2002).
- [20] M. J. Alava and K. Niskanen, *Rep. Prog. Phys* **69**, 669 (2006)
- [21] A. Tanguy, M. Gounelle, and S. Roux, *Phys. Rev. E* **58**, 1577 (1998).
- [22] O. Duemmer and W. Krauth, *J. Stat. Mech.* **P01019** (2007).
- [23] Y. Yu and P. Kärenlampi, *J. Mat. Sci.* **32**, 6513 (1997).
- [24] J. Weiss and D. Marsan, *Science* **299**, 89 (2003).
- [25] Y. Y. Kagan and L. Knopoff, *J. Geophys. Res.* **86** (B4), 2853 (1981).
- [26] T. Utsu, Y. Ogata, and S. Matsuura, *J. Phys. Earth* **43**, 1 (1995).
- [27] A. Helmstetter, D. Sornette, *Phys. Rev. E* **66**, 061104 (2002).
- [28] A. Helmstetter, D. Sornette and J.R. Grasso, *J. Geophys. Res.* **108** (B1), 2046 (2003).

- [29] A. Corral, Phys. Rev. Lett. **92**, 108501 (2004).
- [30] G. Molchan, Pure Appl. Geophys. **162** 1135 (2005).
- [31] S. Hainzl and Y. Ogata, J. Geophys. Res. **110** (B05), S07 (2002).
- [32] A. Saichev and D. Sornette, J. Geophys. Res. **112** (B04), 313 (2007).
- [33] J. Davidsen, S. Stanchits, and G. Dresen, Phys. Rev. Lett. **98**, 125502 (2007).
- [34] D. Bonamy, L. Ponson, S. Prades, E. Bouchaud, and C. Guillot, Phys. Rev. Lett. **97**, 135504 (2006).